Identification of a new inhibitor of Ran GTPase with therapeutic value in epithelial ovarian cancer

Zied Boudhraa[δ,1,2], Xiaohong Tian[δ,5], Sabrina Ritch[ξ,1,2], Ryhem Gam[ξ,1,2], Jennifer Kendall-Dupont[1,2], Euridice Carmona[1,2], Diane Provencher[1,2,3], Jian Hui Wu[5], Anne-Marie Mes-Masson[1,2,4*]

[1] Centre de recherche du Centre hospitalier de l'Université de Montréal (CRCHUM), Montreal, Canada.

[2] Institut du cancer de Montréal (ICM), Montreal, Canada.

[3] Division of Gynecologic Oncology, Université de Montréal, Montreal, Canada.

[4] Department of Medicine, Université de Montréal, Montreal, Canada.

[5] Lady Davis Institute, Jewish General Hospital, McGill University, Montreal, Canada

[δ] First Co-authors

[ξ] Second Co-authors

[*] **Corresponding author:** Anne-Marie Mes-Masson, CRCHUM, R10-412, 900 rue St-Denis, Montreal, Quebec, Canada, H2X 0A9. Phone: (514) 890-8000 ext. 25496. E-mail: anne-marie.mes-masson@umontreal.ca

ABSTRACT

Accumulated studies suggest that the small GTPase Ran is critical in cancer initiation and progression. Compounds that block Ran activity would be valuable for cancer treatment. Here, by learning lessons from the discovery of KRAS G12C inhibitors, we generated a structural model of the switch II pocket of GDP-bound Ran to identify potential inhibitors of Ran by virtual screening. After in vitro verification and hit optimization, we identified chemical compound M36 as an efficient inhibitor of Ran with a therapeutic value. Binding of M36 to Ran was confirmed by cellular thermal shift assay. The specificity of M36 towards Ran was demonstrated by the evaluation of the active GTP-bound forms of a range of GTPases including Ran, RhoA, Cdc42 and Rac1; and by the expression of a dominant active mutant of Ran. Remarkably, similar to depletion of Ran by siRNA, M36 exhibits a specific toxicity in aneuploid ovarian cancer cells and represses DNA repair systems. In accordance with this, we established a synergistic relationship between M36 and the FDA approved PARP inhibitor olaparib. *In vivo*, M36 presents acceptable pharmacokinetic properties and, more importantly, inhibits the tumor growth of an aggressive ovarian xenograft model. Clinically relevant, M36 was able to induce cell death in *ex vivo* EOC patient derived micro-dissected tumors. Overall, our study is the first to provide a small-molecule compound inhibitor of Ran with a therapeutic potential.

INTRODUCTION

Ran (Ras related nuclear protein), a member of the RAS superfamily of small GTPases, is unique among other GTPases owing to its subcellular localization. While other GTPases are found in the cytoplasm and associated to subcellular membranes, Ran is found predominately in the nucleus [1]. Ran has been widely studied for its role in mitosis and nucleo-cytoplasmic shuttling of proteins and RNAs [2]. In comparison with normal tissues, Ran was found to be overexpressed in several cancers including breast, renal, gastric, colon, pancreatic, ovarian and lung cancers [3-10]. Furthermore, within the same cancer the expression of Ran has been found to be positively correlated with patient outcomes in myeloma, lymphoma, neuroblastoma, renal cell, ovarian and breast carcinomas [4-6,10-14]. It has been reported that Ran is involved in supporting at least three hallmarks of cancer, namely proliferative signaling, resisting cell death and activating pathways that support invasion and metastasis [7,9,11,15-21]. Interestingly, we and others have been reported that the loss of Ran using specific siRNAs is lethal for cancer cells with no or moderate effect in normal cells [7,18,22-24]. This suggests that targeting Ran could achieve a valuable therapeutic index.

Epithelial ovarian cancer (EOC) is the most common form of all ovarian cancers and is the most fatal of all gynecological malignancies [25,26]. Histologically, EOCs are subdivided into five subtypes where the high grade serous carcinoma (HGSC) is overrepresented and rates among the most aggressive [25,27]. EOCs are characterized by extremely high intratumoral heterogeneity that poses specific challenges for therapeutic strategies [28] (Platinum- and taxane-based chemotherapy are the standard first-line therapies of EOC [27,29]). However, despite this heterogeneity, aneuploidy is a hallmark of EOC, particularly of HGSC [28] where the chromosomal stability control gene, *TP53*, is mutated in >90% of cases [30,31]. Thus, targeting aneuploidy would be an avenue to efficiently treat this cancer.

43 Recently, we have shown using EOC models, that the differential sensitivity between
44 normal and cancer cells following the loss of Ran is governed by aneuploidy and genomic
45 instability [23]. In particular, we have reported that induction of aneuploidy in rare diploid EOC cell
46 lines or normal cells renders them highly dependent on Ran. We also established an inverse
47 correlation between Ran and the tumor suppressor NR1D1 and reveal the critical role of
48 Ran/NR1D1 axis in aneuploidy-associated endogenous DNA damage repair. We showed that Ran,
49 through the maturation of miR4472, destabilizes the mRNA of NR1D1 impacting several DNA
50 repair pathways [23]. Loss of Ran was then associated with NR1D1 induction, accumulation of DNA
51 damages and lethality of aneuploid EOC cells. Our findings suggest a synthetic lethal strategy
52 targeting aneuploid cells based on their dependency to Ran. We hypothesize that developing small
53 molecules targeting this GTPase is an attractive therapeutic approach for EOC. To date, despite
54 the availability of Ran's crystal structure [32-36], there is no inhibitor proven to be efficient and
55 specific to Ran. The high affinity of Ran to its cognate GTP (pM range) and the high cellular
56 concentration of GTP (millimolar range), makes the identification of an efficient compound with
57 a GTP-competitive mode of action very difficult, if not impossible.

58 In the present study, inspired by the ground-breaking work of KRAS G12C inhibitors[37,38],
59 we aimed to identify allosteric small molecule inhibitors of Ran. The approach chosen was to target
60 the GDP-bound form of Ran at the switch II pocket, with the hypothesis that this would lock the
61 protein in an inactive state, thereby depleting the active Ran population. To this end, a part of the
62 NCI chemical database (90,000 compounds) was screened virtually. After *in vitro* validation and
63 hit optimization, we identified M36 as a promising inhibitor of Ran. M36 mimics the effect of Ran
64 knock down (KD): specific toxicity in aneuploid cancer cells and significant repression of the DDR
65 process. *In vivo*, M36 is well tolerated by mice at high doses, displays an acceptable

66 pharmacokinetic (PK) pattern and significantly delays tumor growth of a very aggressive EOC
67 xenograft model. At the clinical level, M36 was able to induce cell death in *ex vivo* micro-dissected
68 tumors derived from an EOC patient. Furthermore, owing to its ability to repress DNA repair
69 systems, we established a synergistic relationship between M36 and the FDA approved PARP
70 inhibitor olaparib. Overall, our findings suggest a new therapeutic strategy for EOC based on the
71 modulation of Ran activity.

72

73 **RESULTS**

74 ***In silico* and cell-based screenings identified M26 as hit compound for Ran inhibition**

75 Inspired by the ground-breaking work of KRAS G12C inhibitors, which bind KRAS G12C mutant
76 at a pocket nearby switch II (referred to as switch II pocket) [37,38], we aimed to target the GDP-
77 bound form of Ran (RanGDP) at the switch II pocket to 'arrest' Ran at its inactivated state (**Figure**
78 **1A**). However, one key feature of the switch II pocket of KRAS G12C is that it exists only when
79 it binds with an inhibitor. Our inspection of the crystal structure of RanGDP (pdb: 3ch5) found no
80 pre-formed switch II pocket. We thus decided to construct a structural model of the switch II
81 pocket of RanGDP using the crystal structure of KRAS G12C/Inhibitor complex (pdb: 5v6s) as
82 the template **(Figure 1A)**. Next, a part of the NCI chemical database (90,000 compounds) was
83 screened virtually against the RanGDP switch II pocket. Top-ranking compounds identified in this
84 *in silico* screen went through a more in-depth visual inspection for binding modes. A total of 28
85 compounds were selected for further study as potential Ran inhibitors (**Figures 1B and S1A**).
86 Having previously established that aneuploid EOC cells are more sensitive to the loss of Ran than
87 normal or tumoral diploid cells [23], biological activity was assessed by clonogenic assays (at a single
88 dose of 10 μM) using one aneuploid EOC cell line (TOV112D) and the diploid normal ARPE

89 (ARPE-19) cells **(Figures 1C and S1B)**. The criterion for a positive hit was that the compound
90 did not inhibit the colony formation of the ARPE cells but significantly inhibited the number of
91 colonies formed by the TOV112D cells. Our results show that one compound from the *in silico*
92 screening, M26 **(Figure 1B)**, inhibited colony formation of EOC but not the normal cells **(Figure**
93 **1C)**. Furthermore, by analyzing PARP cleavage by Western blot, we found that M26 treatment
94 induced apoptosis in TOV112D cells with no notable effect in ARPE cells **(Figure 1D)**, indicating
95 a differential sensitivity between the diploid and aneuploid cells following M26 treatment. Since
96 our screening was virtual using Ran crystal structure, it was therefore important to determine
97 whether our hit compound was able to inhibit Ran in its biological form. For that, the level of
98 active GTP-bound Ran was evaluated in lysates of EOC cells treated or not with M26 using Ran
99 pull down assays. Our results showed a marked decrease in Ran-GTP level in TOV112D cells
100 incubated with this compound compared to DMSO-treated control cells **(Figure 1E)**. Of note,
101 since the number of cells used in the colony formation assay is lower than that of other cell-based
102 assays, a lower concentration of M26 (or its derivatives, see below) was used in this assay.
103 Collectively, our data identified M26 as a potential inhibitor of Ran with an interesting therapeutic
104 value.

105 **Chemical optimization and cell-based screening identified M36 as a promising inhibitor of**
106 **Ran**

107 Plasma esterases are the major drug-metabolizing enzymes in plasma significantly affecting drug
108 stability *in vivo* [39]. As shown in **Figure 1B**, M26 has three ester groups, which would suggest poor
109 bioavailability of the drug when injected *in vivo*. To overcome this issue and explore preliminary
110 structure-activity relationship, a series of M26-derived compounds, in which the ester groups were
111 replaced by ether groups, were synthetized **(Figures 2A and S2A)**. Our results showed that only

112 compound M36 and its derivative M98, inhibited colony formation of TOV112D cells without
113 affecting the ARPE cells **(Figure S2B)**. Interestingly, M36 but not M33 inhibited the activation of
114 Ran comparably to the parent compound, M26 **(Figure S2C)**. Therefore, for the rest of the study
115 we selected M36 **(Figure 2A)** for further characterization. Using Ran pull down assays, the effect
116 of M36 on Ran activation was shown to be dose dependent **(Figure 2B)**. In addition,
117 immunofluorescence studies using an antibody specific to active Ran-GTP showed no detectable
118 levels of Ran-GTP in TOV112D cells treated with M36 as compared to the intense staining of the
119 DMSO-treated cells **(Figure 2C)**. More importantly the direct binding of M36 to RanGTPase was
120 assessed by CETSA, a widely used technique to verify the interaction of a compound with its target
121 protein.[40] In this assay, the thermal stability of Ran was investigated at different temperatures in
122 OV1946 cells treated with M36 or DMSO **(Figure 2D)**. As expected, Ran levels detected by
123 Western-blot decreased exponentially with increasing temperatures in controls cells treated with
124 vehicle DMSO. However, a right shift in this thermal stability curve was observed when cells were
125 treated with 100 μM M36, and significantly higher levels of Ran were observed at temperatures
126 of 52°C, 55°C and 64.5°C **(Figure 2D)**, indicating M36 engages with Ran and increases its thermal
127 stability. To test the effect of different concentrations of M36 on CETSA, the temperature of 64°C
128 was chosen because it is in the exponential phase of the curve. Our results show a concentration-
129 dependent protection of Ran when cells were treated with M36 **(Figure 2E)**. As negative control,
130 we show that this protection was not observed when OV1946 cells were treated with increasing
131 concentrations of the PARP inhibitor Olaparib (**Figure S3A**), a drug known to impact DNA repair
132 [41]. In all, these results indicate that M36 targets Ran and inhibits Ran-GTP activation.

133 Regarding its effect on cancer cells, the IC_{50} value of M36 for the TOV112D cell line as determined
134 by clonogenic assay was found to be 10.02±0.36 μM. Only a minimal effect was observed for the

135 normal ARPE cell line at high concentrations **(Figure 3A)**. To support our observation regarding
136 the differential sensitivity between diploid and aneuploid cells with M36 treatment, we expanded
137 our analysis by using, in addition to ARPE and TOV112D cell lines, five aneuploid HGSC cell
138 lines [TOV1946, TOV2295(R), OV1946, OV866(2) and OV4485] and one diploid low-grade
139 serous EOC TOV81D cell line. Proliferation assays were performed on these cell lines after
140 treatment with M36. As a positive control, the same cell lines were transfected with siRan that we
141 have previously characterized for its specificity [21,23]. Remarkably, like siRan, M36 demonstrated
142 a specific toxicity in aneuploid cells with only a moderate effect in normal and EOC diploid cells
143 **(Figure 3B)**. Similarly, this toxicity was accompanied by the induction of apoptosis specifically
144 in aneuploid cells **(Figure 3C)**, highlighting the therapeutic potential of M36. Since aneuploidy
145 and genomic instability are hallmarks of the majority of cancers [42,43], we assessed the toxicity of
146 M36 in other cancer cell lines derived from prostate, gastrointestinal, breast and skin cancers.
147 Strikingly, M36 showed a significant toxicity in all the cell lines tested **(Figure S2D)**. These results
148 suggest that the use of M36 would not be limited to ovarian cancer but could be extended to other
149 tumors. To investigate the specificity of M36 towards Ran, the effect of M36 on the activation of
150 other GTPases (RhoA, Cdc42 and Rac1) was assessed. As shown in **Figure 3D**, no significant
151 effect on the activation of these GTPases was observed when incubated with M36. Furthermore,
152 overexpression of constitutively active (GTP-bound form) Ran^{Q69L} mutant protein [44] mitigated the
153 inhibition of TOV112D cell growth by M36 **(Figure 3E)**. Together, these data provide evidence
154 of the specificity of M36 towards Ran and indicate that this compound acts specifically on the
155 GDP-bound form of Ran.

156 **M36 mimics the effect of Ran knock down (KD) regarding DDR**

157 We have shown that the differential sensitivity between diploid and aneuploid cells following the
158 loss of Ran comes from the involvement of the Ran/NR1D1 axis in modulating DNA repair [23]. In
159 fact, following the loss of Ran, NR1D1 was induced and in turn repressed several DNA repair
160 pathways including the HR and the NHEJ pathways, leading to the accumulation of DNA
161 damages. We first assessed the effect of M36 on NR1D1 expression. As observed following Ran
162 KD, M36 significantly induced the expression of NR1D1 in two aneuploid EOC cell lines
163 (TOV112D and OV1946) **(Figure 4A-B)**. As negative control, we show that NR1D1 expression
164 was not affected when cells were treated with the PARP inhibitor Olaparib **(Figure S3B)**,
165 suggesting that M36 effect on NR1D1 expression is specific. Next, to investigate whether M36
166 was able to repress the DDR process, TOV112D cells were either transfected with siRan or treated
167 with M36 and the DDR components were analyzed by immunofluorescence. Remarkably, in
168 accordance with Ran KD, M36 treatment induced DNA damage accumulation as shown by an
169 increase of p-ɣH2AX foci number **(Figure 4C)** and an inhibition of the HR and the NHEJ
170 pathways, which were assessed respectively by the quantification of Rad51 **(Figure 4D)** and
171 53BP1 **(Figure 4E)** foci formation. Interestingly, since the cytoplasmic staining of 53BP1
172 following M36 treatment was increased **(Figure 4F)**, the inhibition of 53BP1 foci formation by
173 M36 can probably be attributed to the inhibition of the Ran-dependent nuclear import of this
174 protein that has been previously reported [15] and is in accordance with the Ran KD condition
175 **(Figure 4F)**. Collectively, our data demonstrate that M36 mimics the effect of the loss of Ran
176 regarding DDR.

177 **Evaluation of the therapeutic potential of M36 *in vivo***

178 The promising *in vitro* results of M36 led us to initiate *in vivo* analysis of this small molecule
179 inhibitor of Ran. Pharmacokinetic results showed that after a single IP injection (200 mg/kg),

180 plasma levels of M36 detected at our first time point of 5 minutes, reached a peak at 30 minutes
181 (100 μM), remained at around 10 μM after 6 h and is still detectable at 24 h **(Figure 5A)**.
182 Therefore, M36 displayed an acceptable PK pattern. For the tolerance study, M36 was injected IP.
183 daily for a period of three weeks. Our results showed that treated mice continued to gain weight
184 **(Figure 5B)**, suggesting that, even at higher doses (200 mg/kg), M36 was well tolerated. Inhibition
185 of tumor growth was evaluated in the human chemoresistant ovarian cancer xenograft model,
186 TOV112D. As we've previously shown, this xenograft model showed resistance to carboplatin
187 treatment [45]. Furthermore, when mice were treated with the maximum tolerated dose of the PARP
188 inhibitor Olaparib **(Figure 5C)**, no significant effect was observed regarding tumor growth.
189 However, M36 treatment significantly delayed tumor growth of this aggressive model **(Figure 5D-**
190 **E)** and prolonged mouse survival **(Figure 5F)**, highlighting the promising potential of this
191 compound for the treatment of EOCs, particularly for those that are difficult to treat.

192 **M36 induces cell death in *ex vivo* ovarian cancer models**

193 To evaluate the clinical relevance of M36 treatment, the viability of microdissected tumor samples
194 derived from EOC xenografts or patient samples were evaluated *ex vivo* using our microfluidic
195 methodology [46]. Our results show **(Figure 6)** a significant increase in the intensity of cleaved
196 caspase 3 (CC3) staining 72 hs after M36 treatment in both the OV1946 xenograft and the
197 TOV12018G patient tumor models. For the TOV112D xenograft model, this effect was also
198 observed, but no significance was achieved **(Figure S3B)**, and a 50% decrease in the nuclear Ki-
199 67 staining was observed in this model 24 hs post-treatment. These results suggest that M36
200 induces cell death by apoptosis and could decrease cell proliferation in *ex vivo* EOC models,
201 including patient tumor, further corroborating its therapeutic value.

202 **Combination of M36 and Olaparib triggers synthetic lethality in EOC cells**

203 It is presumed that resistance to PARP inhibitor therapy is closely related to the activation of the
204 HR pathway of cancer cells [47]. Therefore, combination treatments of PARP inhibitor with drugs
205 that inhibit the HR pathway would be promising to circumvent this resistance. Based on our finding
206 that M36 was able to repress the HR pathway, we sought to determine whether M36 was able to
207 sensitize ovarian cancer cells to Olaparib. First, we investigated the effect of M36 on the activation
208 of the HR pathway by Olaparib. Our data in two HR proficient BRCA1/2 wild-type (WT) ovarian
209 cancer cell lines (TOV112D, OV866(2)) showed that M36 efficiently inhibited the induction of
210 the HR pathway (assessed by Rad51 foci quantification) by Olaparib **(Figure 7A)**, and this
211 repression was comparable when irradiation was used as an inducer of this DNA repair pathway
212 **(Figure 4E)**. Next, combination treatments of M36 with Olaparib were undertaken in three
213 BRCA1/2 WT and Olaparib resistant-cell lines, namely TOV112D, OV866(2) and OV90 cell
214 lines, together with the normal diploid ARPE cell line. These combinations were performed using
215 increasing concentrations of both drugs (all concentrations used are below the IC_{50}) and evaluated
216 using the Bliss independent model [48], in which values below -1 indicate antagonism, values
217 between -1 and 1 indicate additive effects and values above 1 indicate synergy. Remarkably, in
218 contrast to ARPE cells that did not respond to any combination condition, M36 displayed a potent
219 synergistic interaction with Olaparib in all 3 EOC cell lines (Bliss scores ranging from 41.02 to
220 78.6) **(Figure 7B-D)**. Similarly, while no effect was observed in ARPE cells, M36/Olaparib
221 combination induced a significant increase of cell death in the EOC cell lines in comparison with
222 single treatments, as assessed by FACS using DRAQ7 staining **(Figure 7E)** and by Western blot
223 using cleaved caspase-3 antibody **(Figure 7F)**. Overall, our data indicate that combining M36 with
224 Olaparib would be an effective combination therapy to counter PARP inhibitor resistance in
225 ovarian cancer.

226

227 **DISCUSSION**

228 The involvement of Ran GTPase in cancer initiation and progression has been discussed for more
229 than a decade [7,8,15-21]. Furthermore, using several *in vitro* and *in vivo* experimental models, Ran
230 has been proposed as a promising therapeutic target of cancer [8,9,14,19,22,23,49]. Recent reports have
231 proposed new strategies to target Ran in the context of cancer therapy. One of them relies on
232 repurposing Pimozide in Ran Targeting [50]. Pimozide was initially identified as a potent antagonist
233 of dopamine receptor D2 (D2R) and used as an antipsychotic drug for the management of
234 schizophrenia and other psychotic disorders. It has been shown that Pimozide inhibits the
235 expression of Ran at the transcriptional level and inhibits breast cancer cell growth *in vitro* and *in*
236 *vivo* [50]. Although this molecule displays an interesting cancer therapeutic value, it is likely that this
237 drug will display severe side effects at the concentrations needed. In fact, it has been shown that
238 mice lacking D2R had impaired motor activity and movement coordination as well as hyperactivity
239 [51]. More importantly, the posology of Pimozide for patients with psychotic disorders is about 0.2
240 mg/Kg/day, however, in the *in vivo* study proposed for breast cancer therapy, mice were treated
241 daily with Pimozide at 20 mg/Kg/day in order to have a significant effect on tumor growth [50].
242 These very high doses of Pimozide will inevitably be an issue in the exploration of this drug in the
243 context of cancer. Another strategy relies on Nano-encapsulation technology (using PLGA-based
244 nanoparticles) of a shRNA targeting Ran [52] or a peptide inhibiting the activation of this GTPase
245 by disrupting the interaction between Ran and RCC1 [53,54]. Such an approach presents many
246 obstacles making its use in clinic very difficult. First, upon entering the circulation, nanoparticles
247 are often coated with opsonin proteins leading to their clearance by macrophages and affecting
248 their pharmacokinetic properties [55]. Second, blood vessels are leaky with fenestrations ranging

249 between 0.2 and 1.2 μm. Since nanoparticles exist in a range of sizes, it is thought that the size of
250 therapeutic nanoparticles should be well below 200 nm [55,56]. However, the NPs used for Ran
251 targeting have a mean diameter of 182–277 nm [53].

252 Here, we aimed to target Ran directly with a new small molecule inhibitor. To date, there
253 is no available drug specific to Ran. One reason for this is the high intracellular concentration of
254 GTP as well as the high affinity of GTP to its cognate GTPase, making the development of an
255 efficient competitor of GTP difficult. Alternatively, it is thought that developing allosteric
256 compounds able to interact with a given GTPase in its GDP-bound form and to lock it on its
257 inactive state is more convenient to attenuate GTPase activity. Inspired by the work of KRAS
258 G12C inhibitors, which bind KRAS G12C mutant at the switch II pocket[37,38], we aimed to target
259 the RanGDP at the switch II pocket to 'arrest' Ran at its inactivated state. However, our inspection
260 of the crystal structure of RanGDP (pdb: 3ch5) found no pre-formed switch II pocket. We thus
261 constructed a structural model of RanGDP switch II pocket by homology modelling and performed
262 in silico screening against the switch II pocket. Chemical optimization of our initial hit m26 lead
263 to compound m36 as a novel Ran inhibitor. Importantly, M36 displays, *in vitro,* a very interesting
264 therapeutic index between normal and cancer cells that is in alignment with our *in vivo* data. In
265 fact, at higher doses, M36 is well tolerated by mice and exhibits a significant toxicity for one of
266 the most aggressive xenograft models, TOV112D, that do not respond to conventional treatments
267 such as Carboplatin and Olaparib therapies. Furthermore, at the clinical level, M36 was able to
268 induce cell death by apoptosis in *ex vivo* micro-dissected tumors derived from an EOC patient.
269 Another advantage of allosteric inhibitors is that they bind to less conserved sites across GTPases
270 and kinases ensuring specificity and avoiding potential severe side effects [57]. In this regard, we
271 have shown that M36 does not influence the activation of other GTPases such as RhoA, Cdc42

272 and Rac1. More importantly, overexpression of a dominant active of Ran rescued the toxicity of
273 M36 highlighting the specificity of our Ran inhibitor.

274 Olaparib has shown promising results for HGSC treatment and was recently approved by
275 the FDA as maintenance therapy for patients harboring BRCA1/2 mutations (HR deficient) [58].
276 This stratification comes from the observation that HR activation is closely linked to non-
277 responsiveness and resistance to PARP inhibitor therapy [47]. Therefore, combination treatment of a
278 PARP inhibitor with drugs that inhibit the HR pathway is actively being exploited in the clinical
279 setting [59,60], and might be effective to induce lethality in HGSC cells. Here, we have shown that
280 M36 induced HR deficiency and dramatically sensitized three BRCA1/2 WT and Olaparib
281 resistant cell lines (TOV112D, OV866(2) and OV90 [61]) to PARP inhibitor therapy. This result is
282 of great interest since it could open new perspectives to circumvent resistance, and possibly to
283 expand PARP inhibitor therapy to patients that are currently excluded. Many cancers are
284 characterized by widespread aneuploidy and genomic instability [42,43]. Hence, targeting these
285 hallmarks would be effective for the development of a new targeted therapy, not only for EOC,
286 but also for a variety of cancers. In our previous work, we have shown that targeting Ran is an
287 effective way to eliminate cancer cells with chromosomal and genomic instability [23]. This
288 prompted us to investigate the therapeutic value of M36 in other cancers. Interestingly, we found
289 that M36 is also toxic in a range of cancer models including prostate, gastrointestinal, breast and
290 skin cancers. These results are encouraging and in future studies we plan to investigate the *in vivo*
291 efficacy of M36 in these models.

292 In conclusion, though further medicinal chemistry optimization is required, our study is the
293 first to provide the generation of a first-in-class compound inhibitor of Ran with a therapeutic
294 potential for cancer in general and EOC in particular.

295

296 **MATERIALS AND METHODS**

297 **Computational modeling and in silico screening**

298 The structural model of RanGDP with switch II pocket was built using crystal structure of RanGDP
299 (pdb: 3ch5) and crystal structure of KRAS G12C in complex with an inhibitor at switch II pocket
300 (pdb: 5v6s) as the templates, by software Modeller (UCSF, CA, USA). Among the 200 models
301 generated, the model with lowest objective function was selected for further work. 90,000
302 compounds from NCI-open database were virtually screened against the switch II pocket of the
303 RanGDP model, using software GOLD (The Cambridge Crystallographic Data Centre,
304 Cambridge, UK).

305 **Medicinal chemistry**

306 28 top-ranking candidate compounds were kindly provided, as a gift, by the Drug Synthesis and
307 Chemistry Branch, Developmental Therapeutics Program, NCI, Bethesda, MD, USA. Initial hit
308 M26 was re-synthesized and characterized by NMR analysis. Chemical optimization of M26,
309 leading to compound M36, is described in the supplemental information.

310 **Cell lines and cell culture**

311 The human EOC cell lines used [TOV81D, TOV112D, OV90, OV866(2), TOV1946, OV1946,
312 TOV2295(R), OV4485] were derived in our laboratory from patients' tumors (TOV) or ascites
313 (OV) [62-65]. All EOC cell lines were maintained in low oxygen at 7% O_2 and 5% CO_2 and grown in
314 OSE medium (Wisent, Montreal, QC) supplemented with 10% FBS (Wisent), 0.5 µg/mL
315 amphotericin B (Wisent) and 50 µg/mL gentamicin (Life Technologies Inc., Burlington, ON). The
316 human retinal epithelial cell line ARPE (ARPE-19) was purchased from American Type Culture
317 Collection (ATCC, Manassas, VA) and maintained in DMEM-F12 (Wisent) medium

318 supplemented with 10% FBS (Wisent), 0.5 μg/mL amphotericin B (Wisent) and 50 μg/mL
319 gentamicin (Life Technologies Inc.).

320 **Small interference RNA (siRNA) treatment**

321 Suspensions of 10^6 cells in 100 μL of nucleofector solution V (Lonza Group Ltd, Basel,
322 Switzerland) were transfected by electroporation with 1.2 nmoles siRNA targeting Ran (J-010353-
323 06, ON-TARGETplus, Dharmacon Thermo Fisher Scientific Inc., Waltham, MA). For each
324 experiment, efficiency of Ran silencing was verified 48 hours after transfection by Western blot
325 analysis. Scramble siRNA (D-001810-02, Dharmacon) was used as a control in all experiments.

326 **Clonogenic survival**

327 Clonogenic assays were performed as previously described [61]. Colonies were counted under a
328 stereo microscope and reported as percent of control. IC_{50} values were determined using Graph
329 Pad Prism 5 software (GraphPad Software Inc., San Diego, CA). Each experiment was performed
330 in duplicate and repeated three times. Sensitivity of the cell lines to small molecule inhibitors of
331 Ran was assessed using a concentration range of 0–40 μM.

332 **IncuCyte cell proliferation phase-contrast imaging assay**

333 Cells (2,000 cells/well) were plated in a 96-well plate. The next day, compounds were added at
334 the indicated concentrations. Following treatment, cell confluence was imaged by phase contrast
335 using the IncuCyte live cell monitoring system (Essen BioScience, Ann Arbor, MI). Frames were
336 captured at day 0 (immediately after treatment) and at the end of the experiment using a 10X
337 objective. For Ran KD experiments, cells were seeded in a 96-well plate (4,000 cells/well) directly
338 after transfection. Cell confluence monitoring started the next day as described above.

339 **Protein preparation and western blot analysis**

340 Cells were lysed with RIPA buffer containing protease inhibitors. Whole cell lysates were run
341 through a Bradford assay (Thermo Fisher Scientific) for protein quantification. Around 25–50 µg
342 of protein was separated by 12.5% SDS-PAGE and transferred onto nitrocellulose membranes.
343 The resultant blots were probed with Ran (1:10 000, sc-271376 Santa Cruz Biotechnology, Dallas,
344 TX), cleaved PARP (1:1000, #9541, Cell Signaling Technology Inc., Danvers, MA), cleaved
345 caspase 3 (1:1000, #9661, Cell Signaling Technology Inc.), GAPDH (1:2500, #2118, Cell
346 Signaling Technology Inc.) or beta-actin (1:50 000, ab6276, Abcam Inc., Toronto, ON, Canada)
347 primary antibodies overnight at 4°C then with peroxidase-conjugated secondary antibodies for 2
348 hours at room temperature. Proteins were detected using enhanced chemiluminescence (Thermo
349 Fisher Scientific).

350 **RT-PCR**

351 The total RNA from TOV-112D or OV1946 cells was isolated using RNeasy Kit (Qiagen®). The
352 total RNA concentration and purity were measured on a NanoDrop™ spectrophotometer. RNA
353 was reverse transcribed using the QuantiTect Reverse Transcription Kit (Qiagen®) according to
354 the manufacturer's protocol. cDNA amplification was performed with SYBR Green PCR master
355 mix (Applied Biosystems®) using the StepOnePlus Real-Time PCR system (Applied
356 Biosystem®). Negative controls were included in all experiments, and actin served as the
357 housekeeping gene. Primers were ordered from Integrated DNA Technologies, Inc:

358 NR1D1:
359 Forward primer: TGGACTCCAACAACAACACAG
360 Reverse primer: GATGGTGGGAAGTAGGTGGG
361 β-actin:
362 Forward primer: CATGTACGTTGCTATCCAGGC
363 Reverse primer: CTCCTTAATGTCACGCACGAT

364 **Cell death analysis by flow cytometry**

365 Cells were treated with M36. Six days after treatment, adherent and floating cells were mixed and
366 incubated 5 minutes at room temperature with DRAQ 7 (ab109202, Abcam Inc). A maximum of
367 30,000 events were counted per condition using the Fortessa flow cytometer (BD Biosciences,
368 Mississauga, ON) and analyzed with the FlowJo software.

369 **Immunofluorescence**

370 M36-treated and control cells grown on coverslips were washed with 1X PBS, fixed in 4%
371 paraformaldehyde and permeabilized with 0.25% Triton X-100 (Sigma-Aldrich Inc.). After
372 blocking (4% BSA and 4% FBS in PBS), coverslips were incubated with anti–RanGTP (26915,
373 NewEastBioscences, diluted 1:100), anti p-γ-H2AX (Ser139) (05-636, EMD Millipore, diluted
374 1:2000), anti-Rad51 (ab213, Abcam, diluted 1:750), anti 53BP1 (NB100-305, Novus Biologicals,
375 diluted 1:2500) and anti-Geminin (10802-1-AP, Proteintech, diluted 1:1000) antibodies in
376 blocking buffer for 2 hours at room temperature. Subsequently, samples were incubated with Cy-
377 5 (1:500, Life Technologies Inc.) and Alexa Fluor 488 (for Geminin) secondary antibodies for 1
378 hour. Coverslips were mounted onto slides using Prolong® Gold anti-fade reagent with DAPI
379 (Life Technologies Inc.). Images were obtained using a Zeiss microscope (Zeiss observer Z1) with
380 a 20X objective. For Rad51 and 53BP1 analysis, cells were transfected with siRan or treated with
381 M36 for 48 hours then gamma-irradiated at 10 Gy and fixed one hour after irradiation. Automated
382 analysis software from Zeiss (AxioVision™, Carl Zeiss) was used for foci counting. In each
383 condition, γ-H2AX, Rad51 and 53BP1 foci were quantified in roughly 400 nuclei.

384 **Cellular Thermal Shift Assay (CETSA)**

385 OV1946 cells (10^7 cells/petri) were seeded in 100 mm × 15 mm petri dish and allowed to attach
386 for 24 h. Then, cells were treated with DMSO or M36 at concentrations from 50 to 200 μM and
387 incubated for 1 h at 37 °C. After incubation, cells were washed, trypsinized and centrifuged for 5

388 minutes at 1200 rpm. Cells were resuspended in HBSS, divided into different aliquots and heated
389 for three minutes at different temperatures using the Biometra TOne PCR (Analytikjena, Jena,
390 Germany). Cell lysates were then obtained by one freeze-thaw cycle in liquid nitrogen (1 min each
391 step) followed by centrifugation at 20,000 × g for 20 min at 4°C. The supernatants were harvested,
392 and SDS-PAGE loading buffer was added before boiling for 5min. Proteins were migrated and
393 blotted into PVDF membranes. Primary antibodies used were: Ran (ab53775, Abcam, 1/5000) and
394 β-Actin (ab6276, Abcam, 1/5000). Proteins were detected by HRP-secondary antibody and the
395 ECL detection kit (Clarity and Clarity Max ECL Western Blotting Substrates from Biorad).
396 Densitometry analyses were conducted using the UV-VIS Spectrophotometer (Thermo Fisher
397 Scientific) and relative intensity of Ran protein was obtained by the ratio over the β-actin band.

398 **Ran, Cdc42, RhoA and Rac1 activation assays**

399 Cells were seeded onto 6-well tissue culture plates in such a way that cell confluence reached
400 approximately 70% the day of the experiment. The day of the experiment cells were treated for 1
401 hour with the indicated compounds prior to protein extraction and quantification. Assays were
402 performed using the Ran, Rac1 activation assay kits (Cell Biolabs) and the RhoA and Cdc42 G-
403 LISA activation assay kits (Cytoskeleton®) according to the manufacturer recommendations.

404 ***In vivo* study**

405 For the PK studies, 6-week-old female CD1 mice (Charles River laboratories, Senneville, QC,
406 Canada) received a single intraperitoneal injection of M36 (200 mg/kg), dissolved in DMSO 10%,
407 Kolliphor® EL 10%, PEG-400 20% and PBS 60%. For each time point (5, 30, 120, 240, 360 and
408 1440 minutes), 3 mice were sacrificed and blood was collected by cardiac puncture. Plasma levels
409 of the compound were measured by mass spectrometry. For the tolerance test, M36 was dissolved
410 as described above and injected intraperitoneally into 6-week-old female NOD.Cg-

411 Rag1^{tm1Mom}Il2rg^{tm1Wjl}/SzJ (NRG) female mice (The Jackson laboratory, Bar Harbor, ME) every
412 day (except on weekends) at 200 mg/kg. During this study, mice were monitored for survival and
413 weight loss/gain. For the tumor xenograft experiment, NRG mice were injected with 10^6
414 TOV112D cells suspended in a mix of 1:1 PBS and matrigel (BD Biosciences) at subcutaneous
415 sites. Treatments with M36 started the following day. Measurements of tumor size were collected
416 at least twice a week until tumors reached limit points (2000 mm3). All animal procedures were
417 performed in accordance with the guidelines for the Care and Use of Laboratory Animals of the
418 CRCHUM and were approved by the Comité institutionnel de protection des animaux (CIPA)
419 (Protocols #C18009AMMs and C22014AMMs).

420 **Micro-dissected tissue (MDT) production, culture and treatment**

421 MDTs were obtained from both ovarian cancer cell xenografts or patient tissue samples. For the
422 xenografts, cell suspensions containing $1x10^6$ cells for TOV112D or $5x10^6$ cells for OV1946 in
423 PBS-Matrigel were injected subcutaneously in NRG female mice. Solid tumours were harvested
424 at volumes between 800 and 1500 mm^3. For patient tissue, samples were collected from patients
425 following informed consent from the Centre hospitalier de l'Université de Montréal (CHUM),
426 Division of Gynecologic Oncology. Samples were processed immediately upon retrieval. The use
427 of human samples was approved by the Comité d'éthique de la recherche du CHUM (CÉR-CHUM,
428 Protocol #BD 04.002).

429 The micro-dissection and loading procedures were adapted from previously published work [46,66].
430 Briefly, both xenograft and patient tumours were sliced into 1cm slices using a scalpel and
431 processed into 350µm slices using a McIlwain™ tissue chopper (Ted Pella©). Tissue slices were
432 kept in Hank's balanced salt solution (HBSS, Wisent) supplemented with 10% FBS, 55 µg/mL of
433 gentamicin and 0.6 µg/mL of amphotericin B. A 500 µm biopsy punch (PUN0500, Zivic

434 instruments) was then used to produce MDTs, spheroidal tissue of approximately 300 µm in
435 diameter. The loading and trapping of MDTs in microfluidic devices were performed as previously
436 described [46]. MDTs were cultured in OSE (xenografts) or Ovarian TumorMACS™ (MILTENYI
437 BIOTEC; patient samples) media supplemented with 10% FBS, 55 ug/mL of gentamicin and 0.6
438 ug/mL of amphotericin B.
439 MDTs were treated with either 100 or 200 µM of M36 in 1% DMSO (Sigma) for 24 or 72hrs
440 continuously. MDTs were then fixed with 10% formalin (Chaptec) and processed following a
441 previously published paraffin-embedding lithography procedure to create micro-dissected tissue
442 microarray (MDTMA) blocks [46].

443 **MDT Immunofluorescence staining and quantification**

444 MDTMA blocks were cut into 4µm sections and put on Matsunami TOMO® hydrophilic adhesion
445 slides (VWR). Slides were stained for KI67 and cleaved-caspase 3 (CC3) to assess proliferation
446 and cell death, respectively, using the *Discovery Ultra* automated stainer (Ventana Medical System
447 inc. (VMSI)). A pan-cytokeratin (CK) antibody was also used to identify the tumour epithelium
448 of the MDTs. Slides were heated at 60˚C for 20 min before staining. Antigen retrieval was carried
449 out with Cell Conditioning 1 solution (VMSI) for 90 min. Mouse anti-KI67 (1:500) (9449S, Cell
450 Signaling), rabbit anti-CC3 (1:200) (9661S, Cell Signaling) and guinea pig anti-pan-CK (1:200)
451 (BP5069, Cedarlane) antibodies were dispensed automatically and slides were incubated for 60
452 minutes at 37˚C. Secondary antibodies, including anti-mouse Alexa 488 (1:250) (A-11001, Life
453 Technologies), anti-rabbit Alexa 750 (1:200) (A-21039, Life Technologies) and anti-guinea pig
454 Alexa 647 (1:200) (706-605-148, Cedarlane) were also dispensed automatically and slides were
455 incubated for 60 minutes at 37˚C. A mounting medium with DAPI (MJS Biolynx inc) was used to
456 stain the nuclei. Slides were scanned at 20x with either an Olympus BX61 (Olympus) or an Aperio

457 Versa 200 (Leica) microscope. IF filters used for DAPI, KI67, CC3 and tumour epithelium were
458 DAPI, Alexa-488, Cy7 and Cy5, respectively. Stained MDTs were quantified using the
459 VisiomorphDP software (VisioPharm, Denmark, http://visiopharm.com). Percent of CC3 staining
460 or nuclear K-67 staining in the cytokeratin positive area were quantified and plotted as bar graphs.

461 **Statistical analysis**

462 Data from at least three independent experiments are presented as the means ± SD. Statistical
463 analyses were done using GraphPad Prism version 10 (GraphPad Sofware Inc., http://
464 graphpad.com). Comparisons were carried out using Student's t-test. Analysis of MDTs was done
465 using Two-way ANOVA followed by Tukey's test. Comparisons of survival curves were
466 performed using log-rank test. A p-value of less than 0.05 was considered statistically significant.

467

468 **ACKNOWLEDGMENTS**

469 We thank Kim Leclerc Désaulniers and Lise Portelance for technical assistances with the animal
470 experiments and biobank specimen procurement, respectively. We acknowledge the CRCHUM
471 animal facility, the ICM Imaging/Live Imaging platform, the Molecular Pathology core facility of
472 the CRCHUM and the CRCHUM Microfluidic platform. A-MM-M and DP are researchers of the
473 CRCHUM/ICM, which receive support from the Fonds de recherche du Québec – Santé (FRQS).
474 ZB was supported by a MITACS fellowship and by the ICM NathalieMoreau Bursary. SR was
475 supported by a studentship from the Canderel Fund of the Institut du cancer de Montréal (ICM).

476

477 **FUNDING**

478 This work was supported by the Canadian Institute for Health Research (CIHR MOP142724 and
479 PJT148642), the Oncopole in collaboration with the FRQS, the Cancer Research Society, Génome

Québec and IRICoR (#265877), and the ICM (Fonds Défi Spyder and Anne-Marie Chagnon). Cell lines as well as patient tissue samples used in this study were provided by the CRCHUM ovarian tumor bank, which is supported by Ovarian Cancer Canada (OCC) and by the Banque de tissus et de données of the Réseau de recherche sur le cancer (RRCancer) of the FRQS affiliated with the Canadian Tumor Repository Network (CTRNet).

AUTHOR CONTRIBUTIONS

ZB, XT, EC, JHW and A-MM-M designed the study. ZB, XT, SR, RG and JK-D performed the experiments. ZB, XT, EC, SR, RG and JK-D analyzed the data. ZB and XT wrote the manuscript. EC, JHW, DP, and A-MM-M supervised the study, provided guidance, and edited the manuscript.

FIGURES

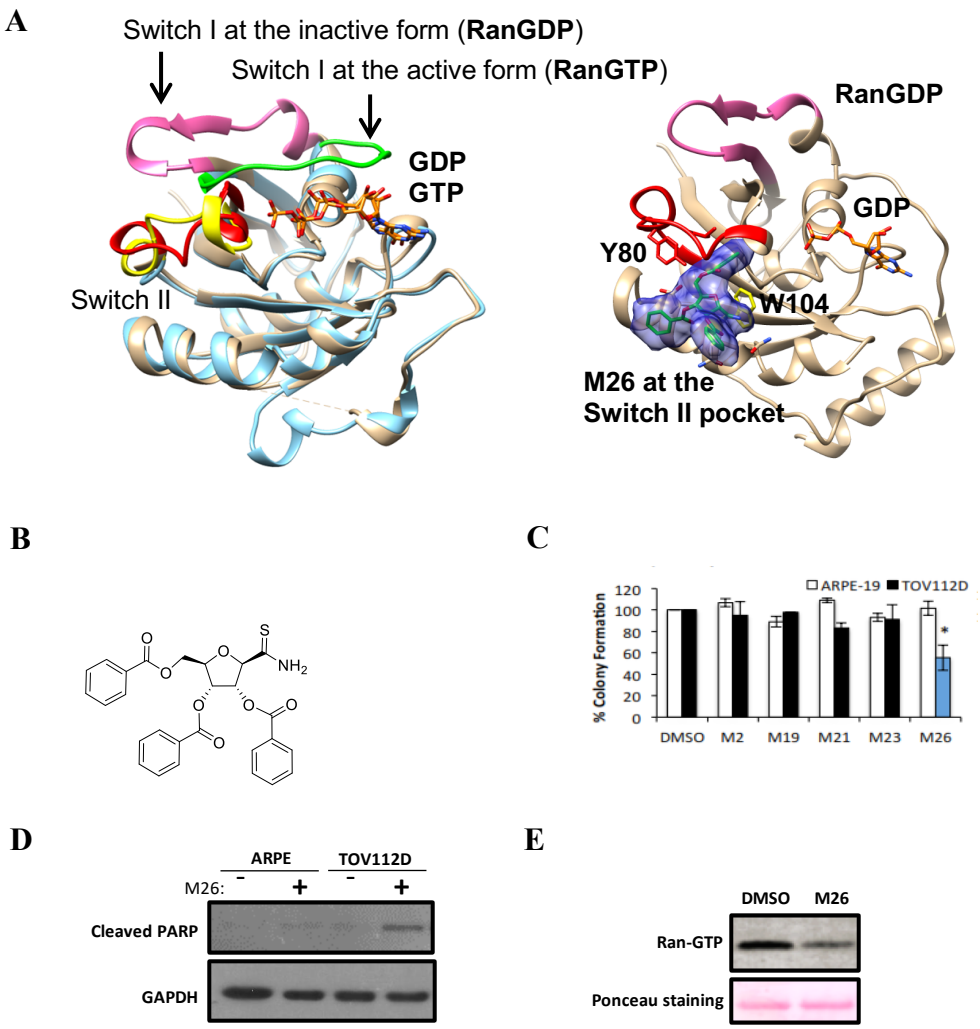

Figure 1: *In silico* and cell-based screenings identified M26 as a hit compound for Ran inhibition.

(A) Left side: Crystal structure of RanGDP (pdb: 3ch5) was aligned to RanGTP (pdb: 3nc1), showing different conformations of Switch I at the activated and inactivated states; Right side: Structural model of the switch II pocket of RanGDP was built by homology modeling and the predicted binding mode of M26 (green sticks with blue surface) at the switch II pocket of RanGDP was showed. **(B)** Chemical structure of M26. **(C)** Colony formation inhibition by selected M compounds at 10 μM in normal ARPE and EOC TOV112D cells. Only the compound M26

503 inhibited TOV112D without affecting ARPE (blue bar). Bars represent percentage of colonies
504 formed compared to DMSO-treated controls. **(D)** ARPE and TOV112D cells were incubated with
505 M26 (40 μM) to evaluate apoptosis (6 days after treatment) by western blot using the antibody
506 anti-cleaved PARP. **(E)** TOV112D cells were incubated for one hour with M26 (50 μM) before
507 performing RanGTP Pull-down assay on the resultant cell extract.
508

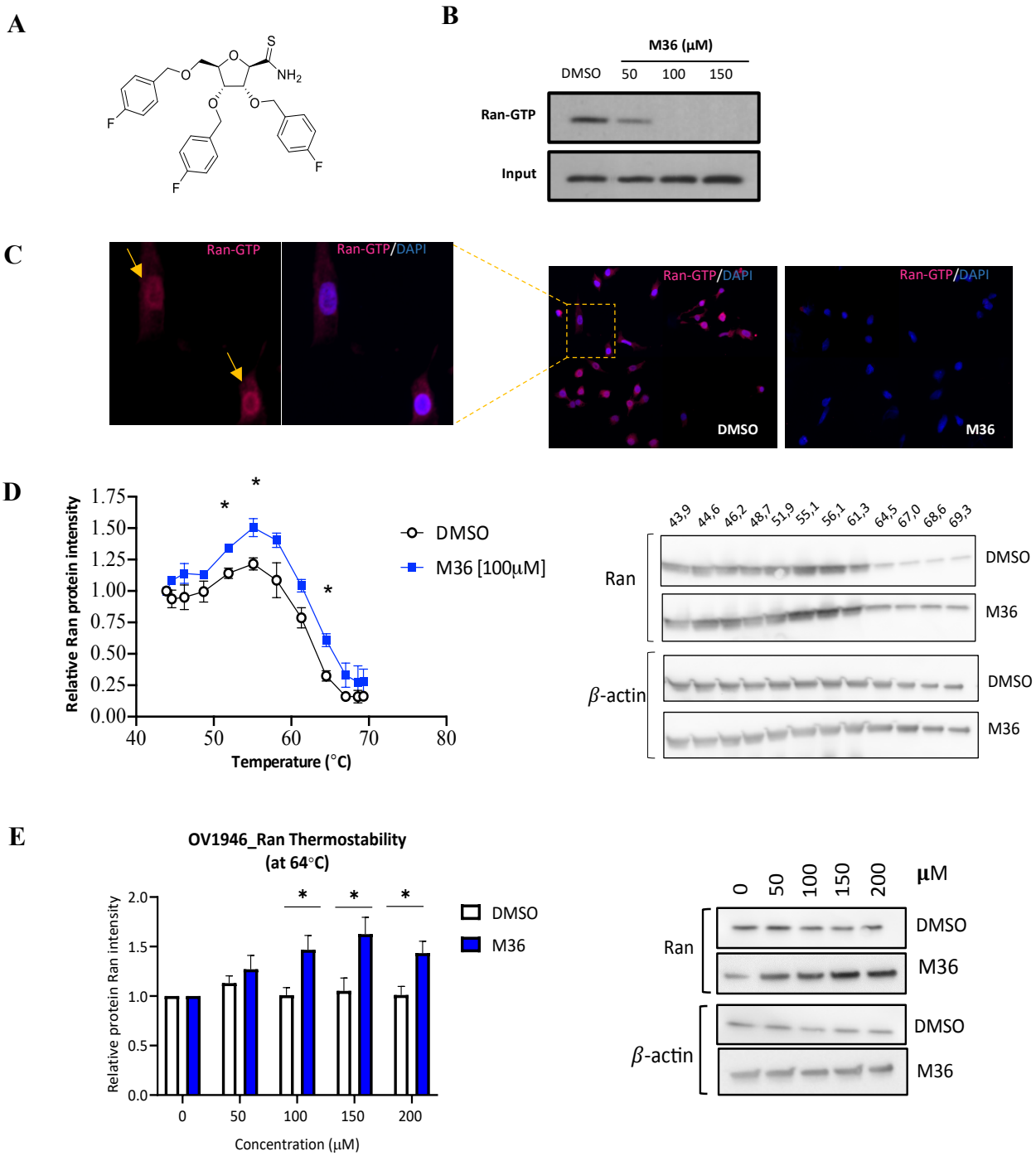

509

510 **Figure 2: M36, a derivative of M26, binds and impacts Ran activation in EOC cells**

511 **(A)** Chemical structure of M36. **(B)** TOV112D cells were treated for one hour with increasing

512 concentrations of M36. Subsequently, RanGTP pull-down assay was performed to assess Ran

513 activation. **(C)** TOV112D cells were treated with M36 (100 μM) for one hour. After cell fixation
514 and permeabilization, RanGTP was revealed by immunofluorescence using a specific antibody
515 (pink). Nuclei are shown by Dapi staining (blue). **(D)** OV1946 cells were treated with M36 (100
516 μM) or DMSO for one hour. CETSA was performed after heating the cell suspensions at different
517 temperatures for three minutes. Cell lysates were subjected to Western blot for evaluation of Ran
518 levels. Data points are densitometry values relative to ß-actin control and normalized to the levels
519 obtained at the lowest temperature used. **(E)** OV1946 cells were treated for one hour with DMSO
520 or increasing concentrations of M36 and CETSA was performed at 64 °C for three minutes and
521 Ran levels were measured by Western blot. Bar graphs represent densitometry values relative to
522 ß-actin control and normalized to the levels obtained for the untreated cells. *$P < 0.05$ ($n = 3$,
523 Student's t-test).
524

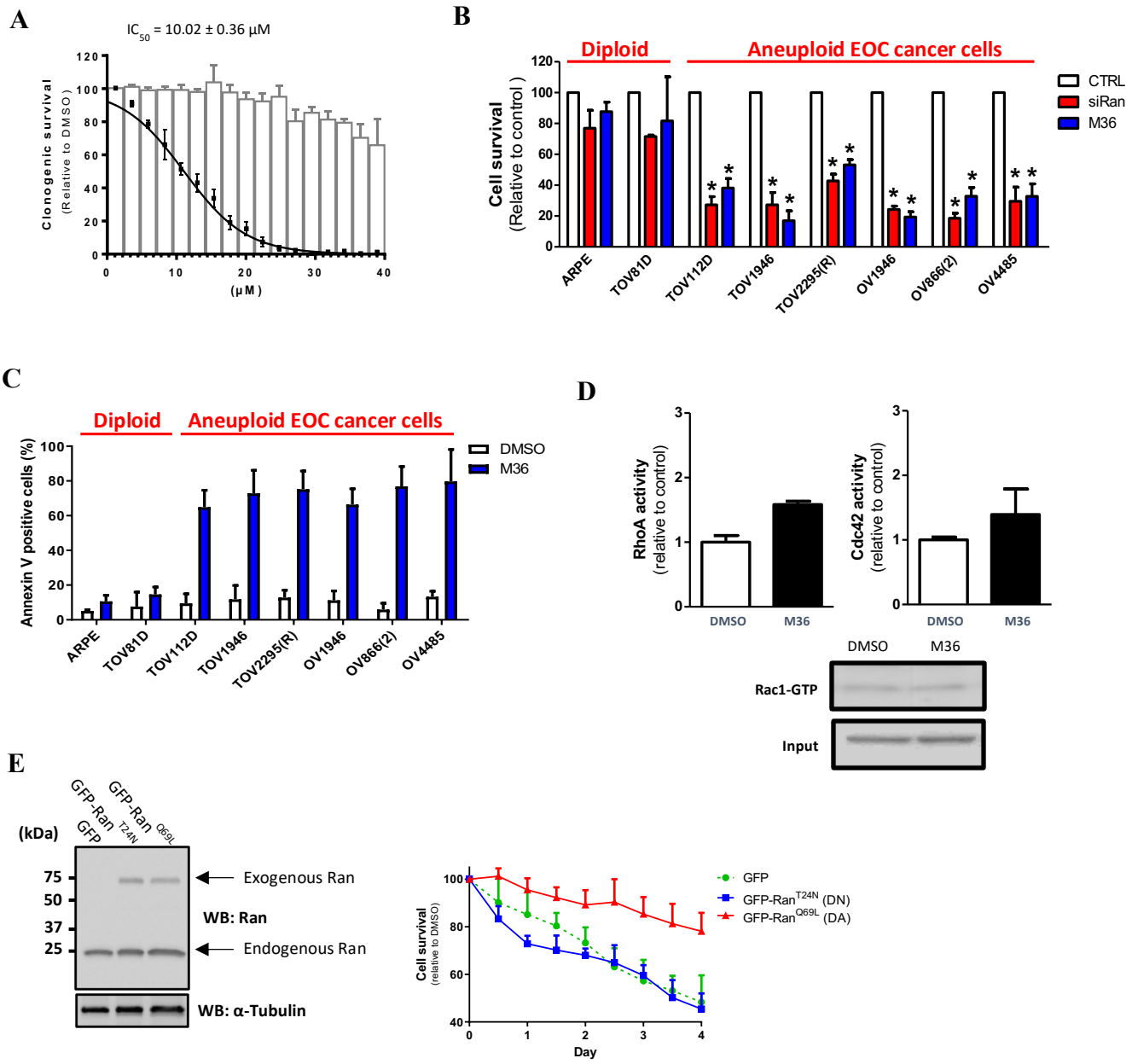

Figure 3: M36 shows selectivity for aneuploid cells and does not interferes with the activation of other GTPases.

(A) Clonogenic assay using different concentrations of M36 in ARPE and TOV112D cells. IC_{50} value was calculated for the TOV112D cells. Bars and curve points represent percentage of colonies formed compared to DMSO-treated controls. **(B)** different EOC cell lines and the normal

531 ARPE cells were transfected with a siRNA targeting Ran or with M36 (40 μM) before assessing
532 cell proliferation using the live cell imaging IncuCyte system. Data are expressed as the percentage
533 of control cells at the end of experiment (96 h) and are representative of at least three independent
534 experiments. **(C)** ARPE and EOC cells were treated with M36 (40 μM) for 6 days and then cell
535 death was assessed by FACS using DRAQ7 staining. **(D)** TOV112D cells were treated for one
536 hour with M36 (50 μM) in order to evaluate RhoA (left), Cdc42 (right) and Rac1 (bottom)
537 activities. **(E)** Immunoblots showing successful overexpression in TOV112D cells of dominant
538 active Ran^{Q69L} and dominant negative Ran^{T24N} (left panel). These cells were treated with M36 and
539 cell proliferation was assessed using the live cell imaging IncuCyte system (right panel). Data are
540 expressed as the percentage of DMSO treated cells. *$P < 0.05$ ($n \geq 3$, Student's t-test).
541

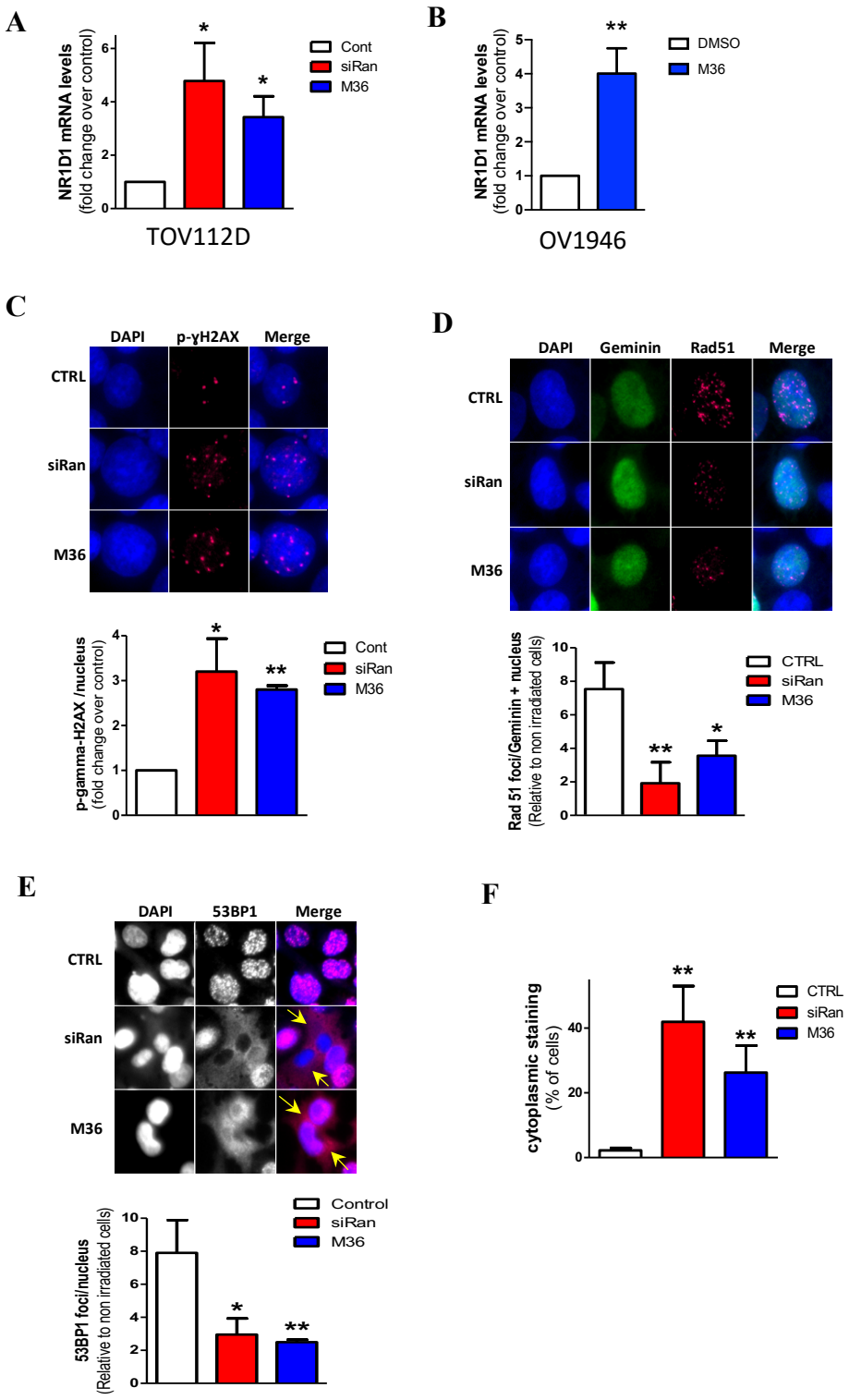

542

543 **Figure 4: M36 mimics the effect of Ran KD regarding DDR**

544 **(A)** The expression of NR1D1 was evaluated by qRT-PCR in TOV112D cells transfected with
545 siRan or treated with M36 (40 μM). **(B)** OV1946 cells were treated with M36 (50 μM) and
546 expression of NR1D1 was evaluated by qRT-PCR. **(C-E)** TOV112D cells were treated with siRan
547 or M36 (20 μM) and allowed to grow for 72 hours. For p-γH2AX staining **(C)**, cells were fixed
548 and stained. For Rad51 **(D)** and 53BP1 **(E)** staining, cells were gamma-irradiated at 10 Gy and
549 fixed 1 hour after irradiation. Representative images after irradiation **(upper panel)** and
550 quantitative analyses of foci formation **(lower panel)** are presented. For Rad51 and 53BP1 foci,
551 data are expressed as the ratio between foci number after and before irradiation. **(F)** Images
552 obtained from **(E)** were used to quantify cells presenting cytoplasmic staining of 53BP1. *$P < 0.05$
553 **$P < 0.01$ ($n \geq 3$, Student's t-test).
554

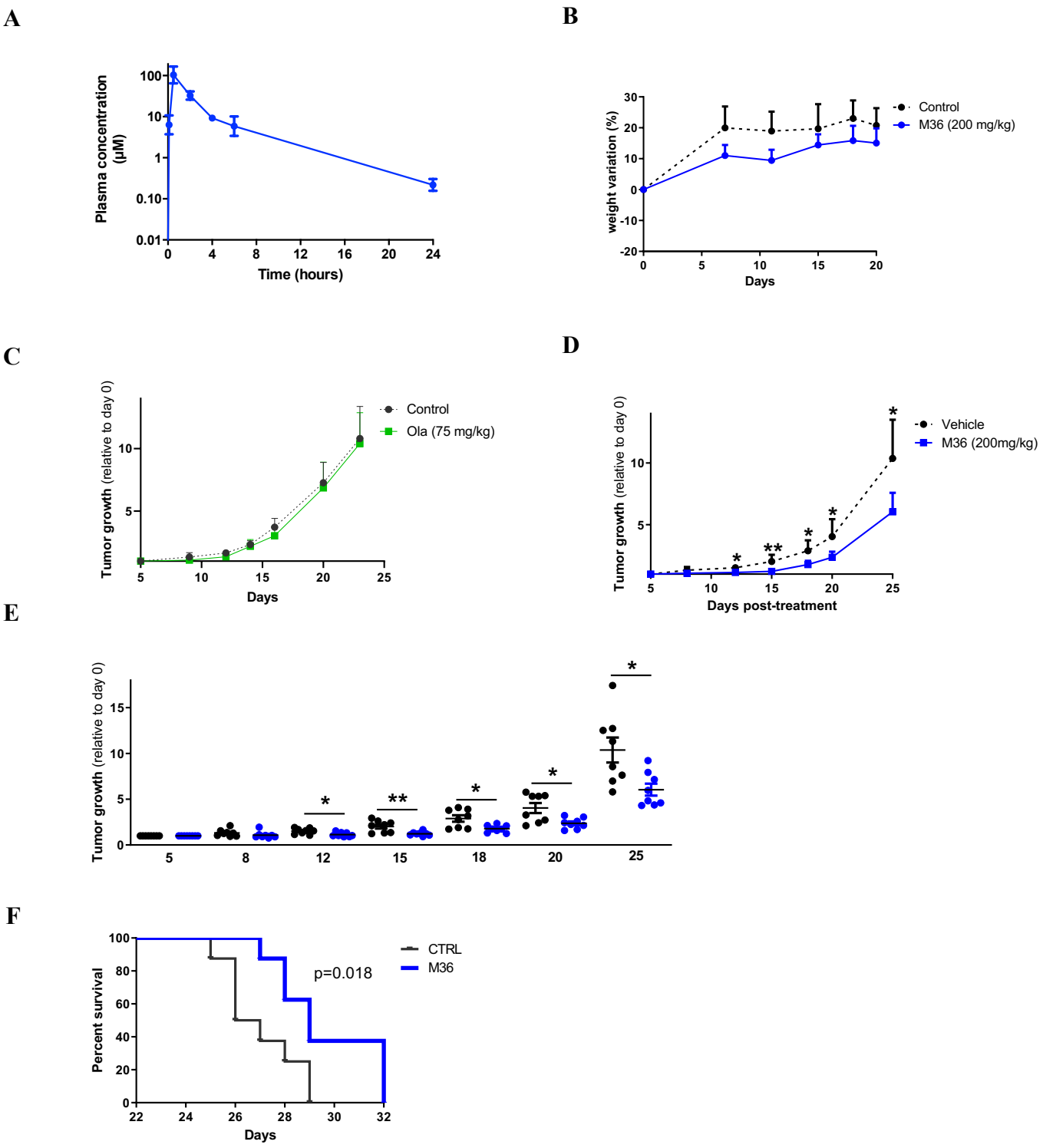

555

556 **Figure 5: Evaluation of the therapeutic potential of M36 *in vivo***

557 **(A)** Measurements of plasma levels of M36 compound after a single intraperitoneal injection (200
558 mg/kg) in CD1 mice. **(B)** M36 (200 mg/kg) was injected IP daily in NRG mice for 3 weeks. Mouse
559 weight was measured at the indicated time points and expressed as the percentage of their weight
560 on the day of the first injection. **(C-D)** TOV112D cells were subcutaneously injected in NRG mice
561 and treatments with Olaparib (75 mg/kg, daily) **(C)**, and M36 (200 mg/kg, daily) **(D)** were
562 performed. Data are normalized with the mean of tumor size at the first day of injection. **(E)** Tumor
563 growth in individual mice treated with M36 is shown. **(F)** Kaplan-Meier survival curve of mice
564 from **(E)**. In **(D)** and **(E)** data were analyzed using the two-tail Student's t test. In **(F)**, data were
565 analyzed using the Log rank test. *$P < 0.05$, **$P < 0.01$.
566

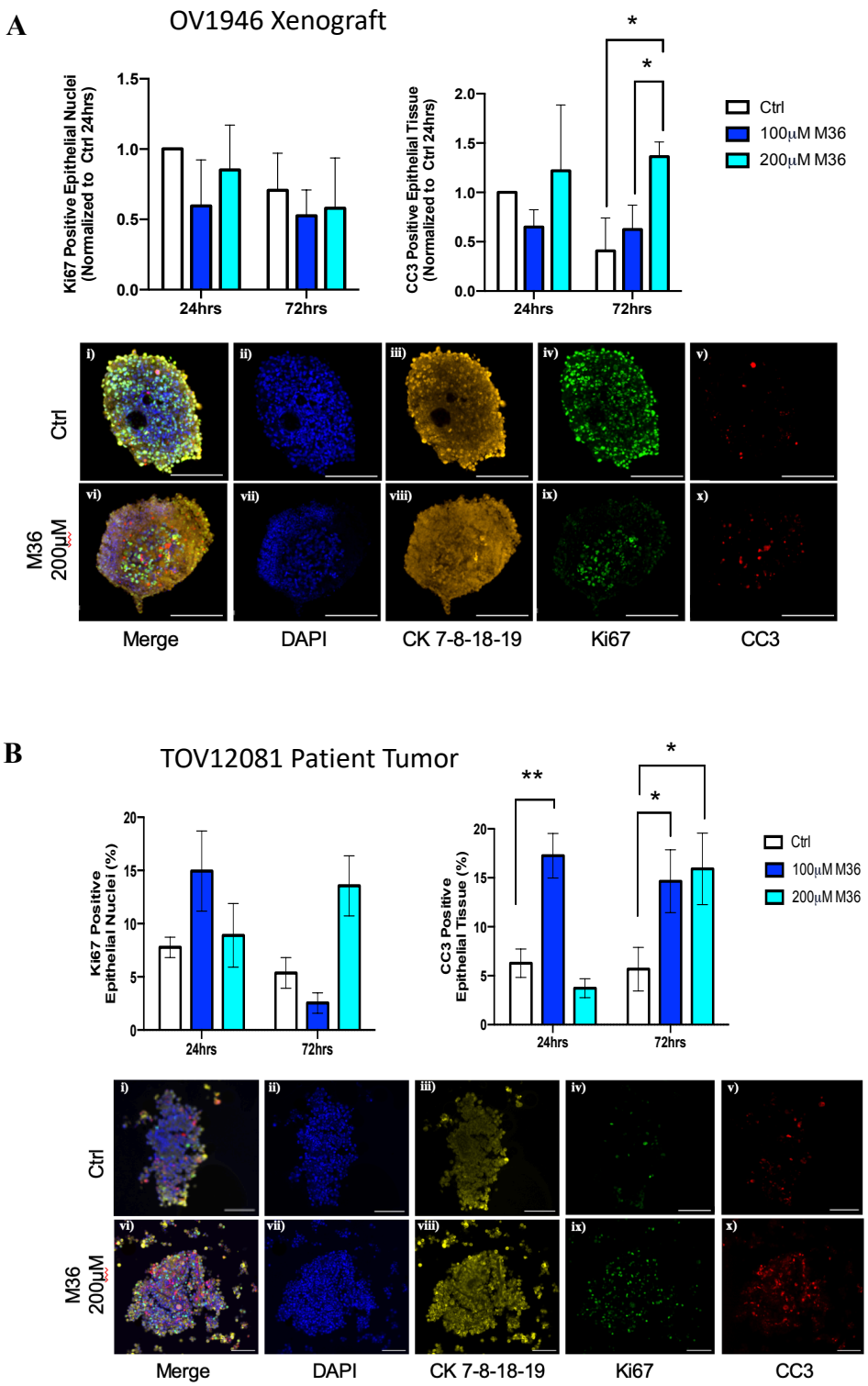

Figure 6: M36 induces cell death of *ex vivo* micro-dissected tumors from xenografts and patients

570 Samples from OV1946 xenografts **(A)** or TOV12018G patient tumor **(B)** were processed as micro-
571 dissected tissues (MDTs) and cultured in microfluidic devices as described in Methods. MDTs
572 were treated with M36 at different concentrations for 24 or 72 h and then formalin-fixed, paraffin
573 embedded. Sections (6μ) were stained for KI67 (green), cleaved-caspase 3 (red), a cytokeratin
574 cocktail (yellow) and DAPI (blue). Bar graphs represent the expression of nuclear KI67 (left
575 panels) or CC3 (right panels) within the tumour epithelium (CK positive cells) of each MDT. Data
576 shown represents mean ± SEM of three separate experiments, normalized to Ctrl 24hrs. Statistical
577 analysis was done using Two-way ANOVA followed by Tukey's test. *$P < 0.05$. Scale bars of
578 representative images are 200 μm.
579

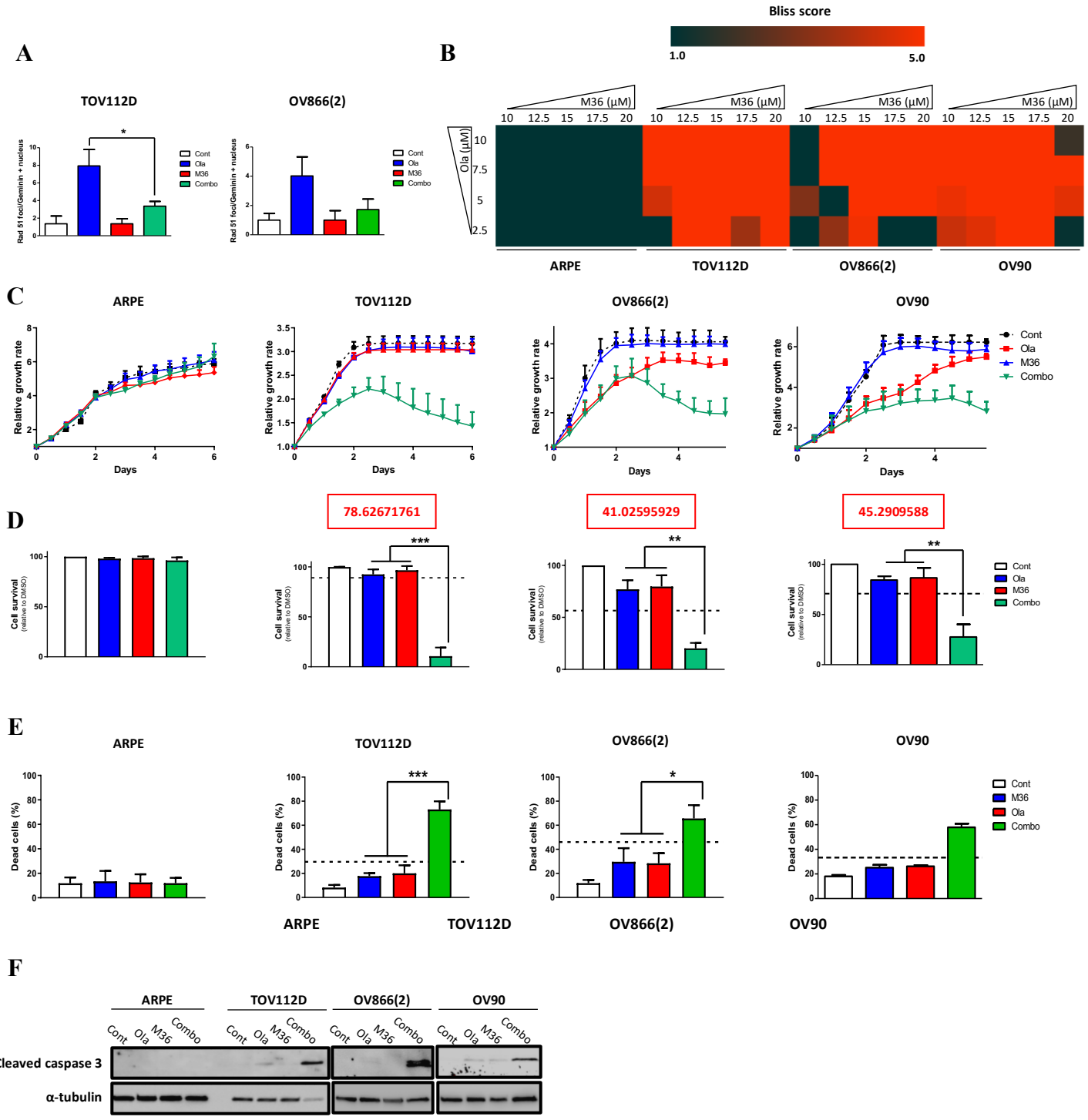

Figure 7: Combination of M36 and Olaparib triggers synthetic lethality in EOC cells

(A) TOV112D and OV866(2) cells were treated with M36 (20 µM) for 48 hours then with Olaparib (10 µM) for 24 hours. After fixation, cells were immunostained with Rad51 antibody. Quantitative

584 analyses of foci formation are presented. **(B)** Cells were treated with increasing concentrations of
585 M36 and/or Olaparib. The heat map shows Bliss scores calculated for each combination at day 6.
586 **(C)** For each cell line, an example of proliferation profile following Olaparib and M36 combination
587 treatment is presented. **(D)** At the end of the experiment presented in **(C)**, dead cells were removed
588 by PBS washes and cell confluence was measured using the live cell imaging IncuCyte system.
589 Data are expressed as the percentage of control cells. **(E, F)** ARPE and EOC cells were treated as
590 in **(C)** and apoptosis was assessed by flow cytometry **(E)** and western blot **(F)** using DRAQ7 dye
591 and cleaved caspase 3 antibody, respectively. *P < 0.05 **P < 0.01 *** P < 0.001 (n = 3. Student's
592 t-test).

593

594 **REFERENCES**

595 1 Matchett, K. B. *et al.* Ran GTPase in nuclear envelope formation and cancer metastasis. *Adv Exp*
596 *Med Biol* **773**, 323-351, doi:10.1007/978-1-4899-8032-8_15 (2014).
597 2 Cavazza, T. & Vernos, I. The RanGTP Pathway: From Nucleo-Cytoplasmic Transport to Spindle
598 Assembly and Beyond. *Front Cell Dev Biol* **3**, 82, doi:10.3389/fcell.2015.00082 (2015).
599 3 Azuma, K. *et al.* Ran, a small GTPase gene, encodes cytotoxic T lymphocyte (CTL) epitopes
600 capable of inducing HLA-A33-restricted and tumor-reactive CTLs in cancer patients. *Clin Cancer*
601 *Res* **10**, 6695-6702, doi:10.1158/1078-0432.CCR-04-0818 (2004).
602 4 Ouellet, V. *et al.* Tissue array analysis of expression microarray candidates identifies markers
603 associated with tumor grade and outcome in serous epithelial ovarian cancer. *Int J Cancer* **119**,
604 599-607, doi:10.1002/ijc.21902 (2006).
605 5 Ouellet, V. *et al.* Discrimination between serous low malignant potential and invasive epithelial
606 ovarian tumors using molecular profiling. *Oncogene* **24**, 4672-4687, doi:10.1038/sj.onc.1208214
607 (2005).
608 6 Abe, H. *et al.* High expression of Ran GTPase is associated with local invasion and metastasis of
609 human clear cell renal cell carcinoma. *Int J Cancer* **122**, 2391-2397, doi:10.1002/ijc.23400 (2008).
610 7 Xia, F., Lee, C. W. & Altieri, D. C. Tumor cell dependence on Ran-GTP-directed mitosis. *Cancer*
611 *Res* **68**, 1826-1833, doi:10.1158/0008-5472.CAN-07-5279 (2008).
612 8 Yuen, H. F. *et al.* Ran is a potential therapeutic target for cancer cells with molecular changes
613 associated with activation of the PI3K/Akt/mTORC1 and Ras/MEK/ERK pathways. *Clin Cancer*
614 *Res* **18**, 380-391, doi:10.1158/1078-0432.CCR-11-2035 (2012).
615 9 Deng, L. *et al.* Ran GTPase protein promotes metastasis and invasion in pancreatic cancer by
616 deregulating the expression of AR and CXCR4. *Cancer Biol Ther* **15**, 1087-1093,
617 doi:10.4161/cbt.29217 (2014).
618 10 Sheng, C. *et al.* Knockdown of Ran GTPase expression inhibits the proliferation and migration of
619 breast cancer cells. *Mol Med Rep* **18**, 157-168, doi:10.3892/mmr.2018.8952 (2018).

620 11 Boudhraa, Z., Carmona, E., Provencher, D. & Mes-Masson, A. M. Ran GTPase: A Key Player in
621 Tumor Progression and Metastasis. *Front Cell Dev Biol* **8**, 345, doi:10.3389/fcell.2020.00345
622 (2020).
623 12 Harousseau, J. L., Shaughnessy, J., Jr. & Richardson, P. Multiple myeloma. *Hematology Am Soc*
624 *Hematol Educ Program*, 237-256, doi:10.1182/asheducation-2004.1.237 (2004).
625 13 Hartmann, E. *et al.* Five-gene model to predict survival in mantle-cell lymphoma using frozen or
626 formalin-fixed, paraffin-embedded tissue. *J Clin Oncol* **26**, 4966-4972,
627 doi:10.1200/JCO.2007.12.0410 (2008).
628 14 Schnepp, R. W. *et al.* A LIN28B-RAN-AURKA Signaling Network Promotes Neuroblastoma
629 Tumorigenesis. *Cancer Cell* **28**, 599-609, doi:10.1016/j.ccell.2015.09.012 (2015).
630 15 Cekan, P. *et al.* RCC1-dependent activation of Ran accelerates cell cycle and DNA repair,
631 inhibiting DNA damage-induced cell senescence. *Mol Biol Cell* **27**, 1346-1357,
632 doi:10.1091/mbc.E16-01-0025 (2016).
633 16 Kurisetty, V. V. *et al.* RAN GTPase is an effector of the invasive/metastatic phenotype induced by
634 osteopontin. *Oncogene* **27**, 7139-7149, doi:10.1038/onc.2008.325 (2008).
635 17 Ly, T. K. *et al.* Activation of the Ran GTPase is subject to growth factor regulation and can give
636 rise to cellular transformation. *J Biol Chem* **285**, 5815-5826, doi:10.1074/jbc.M109.071886 (2010).
637 18 Xia, F., Canovas, P. M., Guadagno, T. M. & Altieri, D. C. A survivin-ran complex regulates spindle
638 formation in tumor cells. *Mol Cell Biol* **28**, 5299-5311, doi:10.1128/MCB.02039-07 (2008).
639 19 Yuen, H. F. *et al.* Ran GTPase promotes cancer progression via Met recepto-rmediated downstream
640 signaling. *Oncotarget* **7**, 75854-75864, doi:10.18632/oncotarget.12420 (2016).
641 20 Yuen, H. F. *et al.* RanGTPase: a candidate for Myc-mediated cancer progression. *J Natl Cancer*
642 *Inst* **105**, 475-488, doi:10.1093/jnci/djt028 (2013).
643 21 Zaoui, K. *et al.* Ran promotes membrane targeting and stabilization of RhoA to orchestrate ovarian
644 cancer cell invasion. *Nat Commun* **10**, 2666, doi:10.1038/s41467-019-10570-w (2019).
645 22 Barres, V. *et al.* An essential role for Ran GTPase in epithelial ovarian cancer cell survival. *Mol*
646 *Cancer* **9**, 272, doi:10.1186/1476-4598-9-272 (2010).
647 23 Boudhraa, Z. *et al.* NR1D1 regulation by Ran GTPase via miR4472 identifies an essential
648 vulnerability linked to aneuploidy in ovarian cancer. *Oncogene* **41**, 309-320, doi:10.1038/s41388-
649 021-02082-z (2022).
650 24 Deng, L. *et al.* Ran GTPase protein promotes human pancreatic cancer proliferation by deregulating
651 the expression of Survivin and cell cycle proteins. *Biochem Biophys Res Commun* **440**, 322-329,
652 doi:10.1016/j.bbrc.2013.09.079 (2013).
653 25 Torre, L. A. *et al.* Ovarian cancer statistics, 2018. *CA Cancer J Clin* **68**, 284-296,
654 doi:10.3322/caac.21456 (2018).
655 26 Siegel, R. L., Miller, K. D., Fuchs, H. E. & Jemal, A. Cancer Statistics, 2021. *CA Cancer J Clin*
656 **71**, 7-33, doi:10.3322/caac.21654 (2021).
657 27 Lheureux, S., Gourley, C., Vergote, I. & Oza, A. M. Epithelial ovarian cancer. *Lancet* **393**, 1240-
658 1253, doi:10.1016/S0140-6736(18)32552-2 (2019).
659 28 Bashashati, A. *et al.* Distinct evolutionary trajectories of primary high-grade serous ovarian cancers
660 revealed through spatial mutational profiling. *J Pathol* **231**, 21-34, doi:10.1002/path.4230 (2013).
661 29 Lheureux, S., Braunstein, M. & Oza, A. M. Epithelial ovarian cancer: Evolution of management in
662 the era of precision medicine. *CA Cancer J Clin* **69**, 280-304, doi:10.3322/caac.21559 (2019).
663 30 Cancer Genome Atlas Research, N. Integrated genomic analyses of ovarian carcinoma. *Nature* **474**,
664 609-615, doi:10.1038/nature10166 (2011).
665 31 Patch, A. M. *et al.* Whole-genome characterization of chemoresistant ovarian cancer. *Nature* **521**,
666 489-494, doi:10.1038/nature14410 (2015).
667 32 Scheffzek, K., Klebe, C., Fritz-Wolf, K., Kabsch, W. & Wittinghofer, A. Crystal structure of the
668 nuclear Ras-related protein Ran in its GDP-bound form. *Nature* **374**, 378-381,
669 doi:10.1038/374378a0 (1995).

670 33 Stewart, M., Kent, H. M. & McCoy, A. J. Structural basis for molecular recognition between
671 nuclear transport factor 2 (NTF2) and the GDP-bound form of the Ras-family GTPase Ran. *J Mol*
672 *Biol* **277**, 635-646, doi:10.1006/jmbi.1997.1602 (1998).
673 34 Chook, Y. M. & Blobel, G. Structure of the nuclear transport complex karyopherin-beta2-Ran x
674 GppNHp. *Nature* **399**, 230-237, doi:10.1038/20375 (1999).
675 35 Vetter, I. R., Arndt, A., Kutay, U., Gorlich, D. & Wittinghofer, A. Structural view of the Ran-
676 Importin beta interaction at 2.3 A resolution. *Cell* **97**, 635-646, doi:10.1016/s0092-8674(00)80774-
677 6 (1999).
678 36 Vetter, I. R., Nowak, C., Nishimoto, T., Kuhlmann, J. & Wittinghofer, A. Structure of a Ran-
679 binding domain complexed with Ran bound to a GTP analogue: implications for nuclear transport.
680 *Nature* **398**, 39-46, doi:10.1038/17969 (1999).
681 37 Ostrem, J. M., Peters, U., Sos, M. L., Wells, J. A. & Shokat, K. M. K-Ras(G12C) inhibitors
682 allosterically control GTP affinity and effector interactions. *Nature* **503**, 548-551,
683 doi:10.1038/nature12796 (2013).
684 38 McGregor, L. M., Jenkins, M. L., Kerwin, C., Burke, J. E. & Shokat, K. M. Expanding the Scope
685 of Electrophiles Capable of Targeting K-Ras Oncogenes. *Biochemistry* **56**, 3178-3183,
686 doi:10.1021/acs.biochem.7b00271 (2017).
687 39 Li, B. *et al.* Butyrylcholinesterase, paraoxonase, and albumin esterase, but not carboxylesterase,
688 are present in human plasma. *Biochem Pharmacol* **70**, 1673-1684, doi:10.1016/j.bcp.2005.09.002
689 (2005).
690 40 Martinez Molina, D. *et al.* Monitoring drug target engagement in cells and tissues using the cellular
691 thermal shift assay. *Science* **341**, 84-87, doi:10.1126/science.1233606 (2013).
692 41 Zeng, Y., Arisa, O., Peer, C. J., Fojo, A. & Figg, W. D. PARP inhibitors: A review of the
693 pharmacology, pharmacokinetics, and pharmacogenetics. *Semin Oncol* **51**, 19-24,
694 doi:10.1053/j.seminoncol.2023.09.005 (2024).
695 42 Levine, M. S. *et al.* Centrosome Amplification Is Sufficient to Promote Spontaneous
696 Tumorigenesis in Mammals. *Dev Cell* **40**, 313-322 e315, doi:10.1016/j.devcel.2016.12.022 (2017).
697 43 Charames, G. S. & Bapat, B. Genomic instability and cancer. *Curr Mol Med* **3**, 589-596,
698 doi:10.2174/1566524033479456 (2003).
699 44 Clarke, P. R., Klebe, C., Wittinghofer, A. & Karsenti, E. Regulation of Cdc2/cyclin B activation
700 by Ran, a Ras-related GTPase. *J Cell Sci* **108 (Pt 3)**, 1217-1225, doi:10.1242/jcs.108.3.1217
701 (1995).
702 45 Brodeur, M. N. *et al.* Carboplatin response in preclinical models for ovarian cancer: comparison of
703 2D monolayers, spheroids, ex vivo tumors and in vivo models. *Sci Rep* **11**, 18183,
704 doi:10.1038/s41598-021-97434-w (2021).
705 46 Simeone, K. *et al.* Paraffin-embedding lithography and micro-dissected tissue micro-arrays: tools
706 for biological and pharmacological analysis of ex vivo solid tumors. *Lab Chip* **19**, 693-705,
707 doi:10.1039/c8lc00982a (2019).
708 47 Lord, C. J. & Ashworth, A. BRCAness revisited. *Nat Rev Cancer* **16**, 110-120,
709 doi:10.1038/nrc.2015.21 (2016).
710 48 Bansal, M. *et al.* A community computational challenge to predict the activity of pairs of
711 compounds. *Nat Biotechnol* **32**, 1213-1222, doi:10.1038/nbt.3052 (2014).
712 49 Xia, Y. *et al.* Increased miR-203-3p and reduced miR-21-5p synergistically inhibit proliferation,
713 migration, and invasion in esophageal cancer cells. *Anticancer Drugs* **30**, 38-45,
714 doi:10.1097/CAD.0000000000000687 (2019).
715 50 Dakir, E. H. *et al.* The anti-psychotic drug pimozide is a novel chemotherapeutic for breast cancer.
716 *Oncotarget* **9**, 34889-34910, doi:10.18632/oncotarget.26175 (2018).
717 51 Anzalone, A. *et al.* Dual control of dopamine synthesis and release by presynaptic and postsynaptic
718 dopamine D2 receptors. *J Neurosci* **32**, 9023-9034, doi:10.1523/JNEUROSCI.0918-12.2012
719 (2012).

720 52 Sharma, A., McCarron, P., Matchett, K., Hawthorne, S. & El-Tanani, M. Anti-Invasive and Anti-
721 Proliferative Effects of shRNA-Loaded Poly(Lactide-Co-Glycolide) Nanoparticles Following
722 RAN Silencing in MDA-MB231 Breast Cancer Cells. *Pharm Res* **36**, 26, doi:10.1007/s11095-018-
723 2555-6 (2018).
724 53 Haggag, Y. A. *et al.* Nano-encapsulation of a novel anti-Ran-GTPase peptide for blockade of
725 regulator of chromosome condensation 1 (RCC1) function in MDA-MB-231 breast cancer cells.
726 *Int J Pharm* **521**, 40-53, doi:10.1016/j.ijpharm.2017.02.006 (2017).
727 54 Haggag, Y. A. *et al.* Novel Ran-RCC1 Inhibitory Peptide-Loaded Nanoparticles Have Anti-Cancer
728 Efficacy In Vitro and In Vivo. *Cancers (Basel)* **11**, doi:10.3390/cancers11020222 (2019).
729 55 Desai, N. Challenges in development of nanoparticle-based therapeutics. *AAPS J* **14**, 282-295,
730 doi:10.1208/s12248-012-9339-4 (2012).
731 56 Haley, B. & Frenkel, E. Nanoparticles for drug delivery in cancer treatment. *Urol Oncol* **26**, 57-64,
732 doi:10.1016/j.urolonc.2007.03.015 (2008).
733 57 Fang, Z., Grutter, C. & Rauh, D. Strategies for the selective regulation of kinases with allosteric
734 modulators: exploiting exclusive structural features. *ACS Chem Biol* **8**, 58-70,
735 doi:10.1021/cb300663j (2013).
736 58 Kim, G. *et al.* FDA Approval Summary: Olaparib Monotherapy in Patients with Deleterious
737 Germline BRCA-Mutated Advanced Ovarian Cancer Treated with Three or More Lines of
738 Chemotherapy. *Clin Cancer Res* **21**, 4257-4261, doi:10.1158/1078-0432.CCR-15-0887 (2015).
739 59 Drean, A., Lord, C. J. & Ashworth, A. PARP inhibitor combination therapy. *Crit Rev Oncol*
740 *Hematol* **108**, 73-85, doi:10.1016/j.critrevonc.2016.10.010 (2016).
741 60 O'Sullivan Coyne, G., Chen, A. P., Meehan, R. & Doroshow, J. H. PARP Inhibitors in Reproductive
742 System Cancers: Current Use and Developments. *Drugs* **77**, 113-130, doi:10.1007/s40265-016-
743 0688-7 (2017).
744 61 Fleury, H. *et al.* Cumulative defects in DNA repair pathways drive the PARP inhibitor response in
745 high-grade serous epithelial ovarian cancer cell lines. *Oncotarget* **8**, 40152-40168,
746 doi:10.18632/oncotarget.10308 (2017).
747 62 Ouellet, V. *et al.* Characterization of three new serous epithelial ovarian cancer cell lines. *BMC*
748 *Cancer* **8**, 152, doi:10.1186/1471-2407-8-152 (2008).
749 63 Fleury, H. *et al.* Novel high-grade serous epithelial ovarian cancer cell lines that reflect the
750 molecular diversity of both the sporadic and hereditary disease. *Genes Cancer* **6**, 378-398 (2015).
751 64 Letourneau, I. J. *et al.* Derivation and characterization of matched cell lines from primary and
752 recurrent serous ovarian cancer. *BMC Cancer* **12**, 379, doi:10.1186/1471-2407-12-379 (2012).
753 65 Provencher, D. M. *et al.* Characterization of four novel epithelial ovarian cancer cell lines. *In Vitro*
754 *Cell Dev Biol Anim* **36**, 357-361, doi:10.1290/1071-2690(2000)036<0357:COFNEO>2.0.CO;2
755 (2000).
756 66 Astolfi, M. *et al.* Micro-dissected tumor tissues on chip: an ex vivo method for drug testing and
757 personalized therapy. *Lab Chip* **16**, 312-325, doi:10.1039/c5lc01108f (2016).

758